Detection and Characterization of Simulated Clandestine Burials Using GPR

Brooks, Kate; Draganov, Deyan; Ngan-Tillard, Dominique; Lüschen, Mark; Nienaber, Coen; Slob, Evert

DOI
10.1109/IWAGPR57138.2023.10329214

Publication date
2023

Document Version
Final published version

Published in
2023 12th International Workshop on Advanced Ground Penetrating Radar, IWAGPR 2023

Detection and Characterization of Simulated Clandestine Burials using GPR

Kate Brooks
Dept. of Geoscience and Engineering
Delft University of Technology
Delft, The Netherlands
katebrooks614@gmail.com

Deyan Draganov
Dept. of Geoscience and Engineering
Delft University of Technology
Delft, The Netherlands
d.s.draganov@tudelft.nl

Dominique Ngan-Tillard
Dept. of Geoscience and Engineering
Delft University of Technology
Delft, The Netherlands
d.j.m.ngan-tillard@tudelft.nl

Mark Lüschen
Central Forensic Service Center
Netherlands National Police
Driebergen, The Netherlands
mark.luschen@politie.nl

Coen Nienaber
Specialist Services & Expertise
Division, Forensic Anthropology and Archeology
The Netherlands Forensic Institute
The Hague, The Netherlands
c.nienaber@nfi.nl

Evert Slob
Dept. of Geoscience and Engineering
Delft University of Technology
Delft, The Netherlands
e.c.slob@tudelft.nl

2023 12th International Workshop on Advanced Ground Penetrating Radar (IWAGPR) | 979-8-3503-3788-4/23/$31.00 ©2023 IEEE | DOI: 10.1109/IWAGPR57138.2023.10329214

***Abstract* — We conducted ground penetrating radar (GPR) surveys to detect the presence of simulated clandestine burials at the Amsterdam Research Initiative for Subsurface Taphonomy and Anthropology (ARISTA) test facility. Our aim is to determine the characteristic responses of the simulated clandestine burials in this man-made sandy environment (reclaimed land) and use them to provide recommendations for forensic investigations. We performed GPR surveys over three simulated clandestine burials at ARISTA during four non-consecutive days. The acquired data represent common-offset data to investigate changes to burial detectability depending on central antenna frequency (250 MHz and 500 MHz), different GPR instruments (NOGGIN or pulseEKKO), changes to survey grid orientation relative to burials, and increased soil moisture content in the survey area. In common-offset radargrams the burial anomalies take on many forms, appearing as disruptions to existing features (direct-wave arrivals and soil horizons) and as isolated reflection events (hyperbolic events and burial-length horizontal anomalies). In time slices, the burials are characterized by high- or low-amplitude rectangular anomalies. When used in conjunction, the radargrams and time slices produce characteristic responses consistent with the locations of the burials, regardless of the survey grid orientation. Increased soil moisture at the site improves the detectability of the burials.**

Keywords — GPR, clandestine, burial, detection, imaging

I. Introduction

Ground penetrating Radar (GPR) is in use as a geophysical tool for forensic investigations since more than 25 years [1]. It has quickly become the most commonly used geophysical technique in forensic investigations. In the past two decades, the number of published case studies using GPR to locate clandestine burials in a forensic context has steadily increased. Typically, antenna frequencies between 400 MHz and 500 MHz are used as they strike a balance between resolution and depth of penetration [e.g., 2], but 110 MHz to 250 MHz antennas have also been used [e.g., 3,4].

The presence of a clandestine burial can be detected due to a contrast in material properties between the grave and/or the body and the surrounding material. Disturbed soil within the grave, or a break in a soil horizon, has been found to generate prominent features in GPR sections, appearing as a high-amplitude horizontal reflection [5]. The target response of clandestine burials in GPR time slices was demonstrated by [5] to form rectangular-shaped anomalies. Non-biological items such as clothing or coverings have been found to increase detectability due to increased material contrast [e.g., 6]. It was shown that skeletonized remains show much lower-amplitude half-hyperbolic reflections as compared to remains in earlier stages of decomposition [5]. Reference [7] found that the largest contributor to the total burial anomaly was the disturbed burial zone rather than the buried body itself, due to the absence of buried artefacts. Moreover, the detectability of clandestine burials is impacted by their relative position with respect to the GPR lines. Reference [8] scanned clandestine burials lengthwise, which showed long dense reflections, while scanned through the chest and abdomen showed a hyperbolic reflection. Target detectability and signature have been found to vary significantly over time due to the decreasing contrast between the surrounding soil and the burial [3]. Favourable environmental conditions for conducting GPR surveys include regions with sandy soils, which are free of debris, flat and level ground, and open areas without dense brush. Detection in sandy soils might be improved by the presence of a diagnostic soil horizon. Non-favourable conditions include soils with high conductivity, i.e., soils which are water-saturated, or have high clay and high organic content. In some cases, added moisture in the soil has been reported to highlight clandestine burials [2].

II. Investigation Site and Instruments

A. Site

We surveyed three burials at the ARISTA test facility. The position and orientation of these burials are shown in the map in Fig. 1. The burials were dug individually and in a standardized way to a size of 1 m x 2 m and to a depth of 0.6 m. They were initially dug for a taphonomy study in which the bodies were exhumed and observed 13 weeks (~ 90 days) following initial burial (PDI). Table 1 lists for each of the three burials the dates of the burial and of the full exhumation and reburial as well as the days since initial burial on the day of each survey. Together with the bodies digital probes were buried, which could be used for monitoring of the subsurface conditions. At the initial burying, the bodies were placed lying on their backs. Contrary to that, during the reburials the bodies were placed in different positions and in different locations in the grave, for example directly against the side of the grave or lying on their side. The current specific situation of each burial is not known. In addition to the listed in Table 1 exhumation and reburials, a number of additional excavations had been carried out for visual observation of degradation and for sampling. E.g., burial C in Fig. 1 was excavated several times and used for training purposes.

To mimic clandestine burials, the soil around the burials is undisturbed, that is, the bases of the burials represent undisturbed compacted soil. The soil itself is made up of marine sand that was brought into the site when the land was reclaimed. After placing the bodies, the dug holes were refilled with their corresponding excavated material. Note that, as a consequence of the multiple excavations, the soil of the burials is clearly distinguishable from the surrounding soil and form low mounds protruding a few centimeters above the surrounding surface (Fig. 1). We can observe in Fig. 1 that the burials are not covered by vegetation due to the agitation of the soil and the prevailing dry weather conditions preceding the data collection.

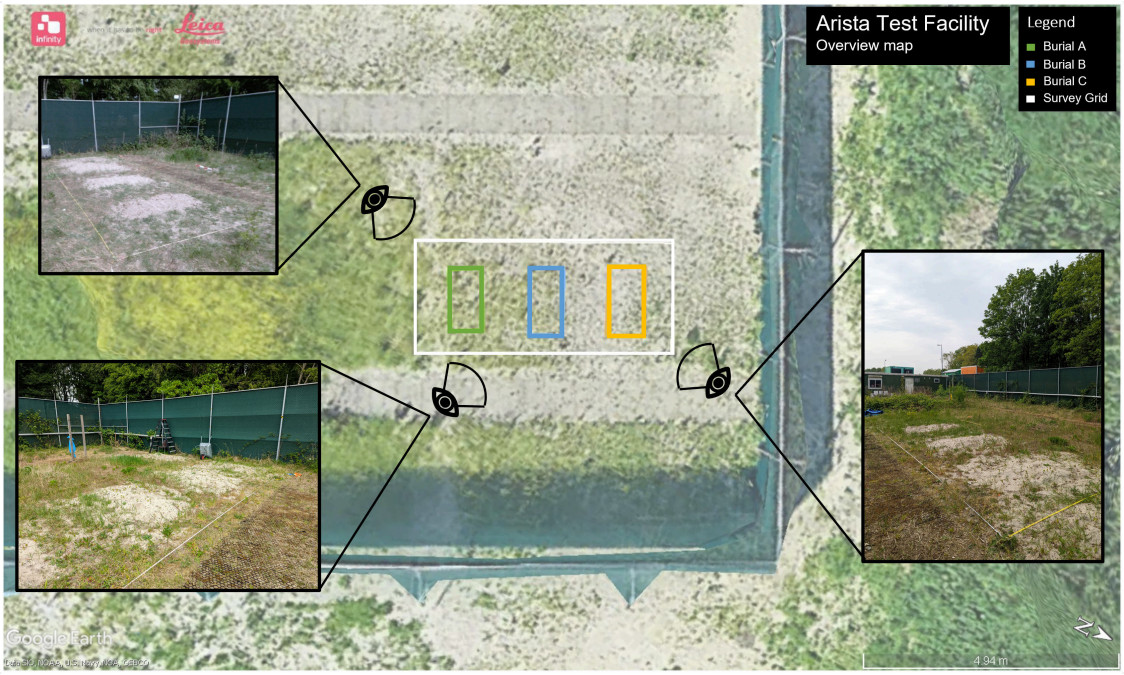

Fig. 1. Overview Map of the ARISTA facility where GPR surveys were performed in this work. The three burials of interest for this study are marked in Green - burial A, Blue - burial B and Orange - burial C. Inset images provide a visual of the burials in their present state, wherein the grave-fill can be clearly differentiated from the surrounding soil.

TABLE I. BURIAL, EXHUMATION AND REBURIAL DATES AND THE RELATIVE AGES SINCE FIRST BURIAL ON SURVEY DAYS.

BURIAL ID	BURIAL	EXHUMATION AND REBURIAL	DAY 1	DAY 2	DAY 3	DAY 4
C	24 SEPT. 2021	23 DEC. 2021	228	243	251	263
B	15 OCT. 2021	13 JAN. 2022	207	222	230	242
A	3 NOV. 2021	2 FEB. 2022	188	203	211	223

B. *Instruments*

We used two instruments - NOGGIN with SmartCart and pulseEKKO with SmartTow from Sensors & Software Inc. For both instruments, we used 250 MHz and 500 MHz shielded antennas to record common-offset surveys on rectangular grids at a fixed spatial step using their odometers. For the NOGGIN instrument, the antennas are located in a single shielding unit with a baseplate with dimensions of 63 x 41 x 23 cm for the 250 MHz and 38 x 23 x 15 cm for the 500 MHz antennas. For the pulseEKKO instrument, the 250 MHz transducer footprint is 30 cm x 30 cm, while the 500 MHz transducer footprint is 15 cm x 15 cm. Line spacing was chosen to be 25 cm for all antennas used. The sampling interval was chosen to be 400 ps for the 250 MHz and 200 ps for the 500 MHz antennas.

III. RESULTS AND INTERPRETATION

First, we show the comparison of the recordings with the two instruments. In Fig. 2 we present radargrams in the space-time (x-t) and space-frequency (x-f) domains acquired with 500-Hz antennas using the NOGGIN (a,c) and pulseEKKO (b,d) along a line perpendicular to the three burials and intersecting them all. In general, the comparison shows the same features, but we can notice several differences. For example, the direct wave Fig. 2a in the NOGGIN data is of much higher amplitude and appears more like a continuous event. Contrary to that, the direct arrival in Fig. 2a in the pulseEKKO data exhibits clearer discontinuities, i.e., jumps in the arrival times along the recorded line. An additional difference between the instrument recordings is that in the x-t domain (Fig. 2a) the pulseEKKO scale bar is skewed towards the negatives, while the NOGGIN is centered at 0 amplitude.

In the x-f domain (Fig. 2b), the amplitude spectrum of the NOGGIN line contains contributions from higher frequencies, with the energy clearly distributed further away from the central frequency 500 MHz – we can see energy up to 2500 MHz. The amplitude spectrum of the pulseEKKO line has the majority of the signals energy concentrated below 500 MHz with almost no energy present above 1000 MHz.

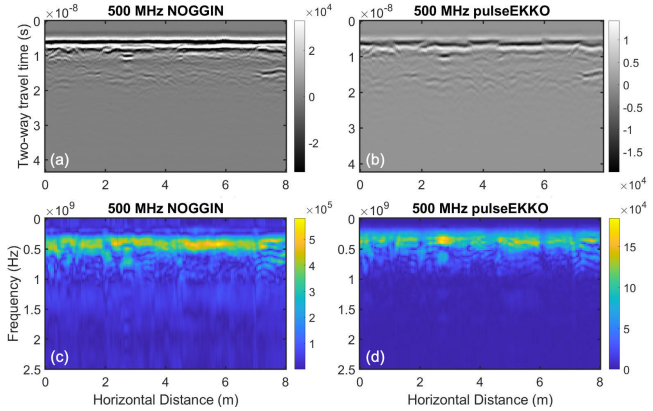

Fig.2 GPR measurements along a line intersecting perpendicularly all three burials recorded with 500 MHz antennas using the (a,c) NOGGIN and (b,d) pulseEKKO instruments depicted in (a,b) space-time domain and (c,d) space-frequency domain. The colour-bars present the amplitude of the recorded signal.

500-MHz radargram for Line x7 has more hyperbolic reflection events across the profile, and, overall, more ringing reflections can be observed compared with the 250-MHz radargram. For Line x7, the hyperbolic reflections are observed on the 500-MHz data with maximum at 10 ns at 1.25 m, 4 m, and 6.75 m, while in the 250-MHz data the only clear hyperbolic reflection is located at approximately 1.25 m, which is consistent with the arrival times in the 500-MHz data. In the 250-MHz radargram along Line x7 we can see clear travel-time jumps for the direct-wave arrival at 1.25 m - 2 m, 3.75 m - 4.75 m, and 6 m - 7 m; these jumps are less pronounced in the 500-MHz radargram. In the data recorded along Line y6 (Figs. 3e,f) there is a strong horizontal, linear feature starting at approximately 1 m and extending to approximately 3 m at 12.5 ns two-way travel time. This feature appears more horizontally continuous in the 250-MHz data than in the 500-MHz data. In the 250-MHz data along Line y6, a hyperbolic feature at 1 m intersects the direct wave at about 5 ns two-way travel time, which is indistinguishable in the 500-MHz data. In the data recorded along Line y22 (Figs. 3h,i), we can observe a clear, nearly continuous linear feature at 12.5 ns travel time which extends nearly along the complete length of the line. In the radargrams along Line y22 the travel-time jumps for the direct-wave arrival are nearly not present compared to jumps present along the other two lines.

In Fig. 4, we compare time slices for the 250-MHz (Fig. 4a,c) and 500-MHz (Fig. 4b,d) data recorded with the

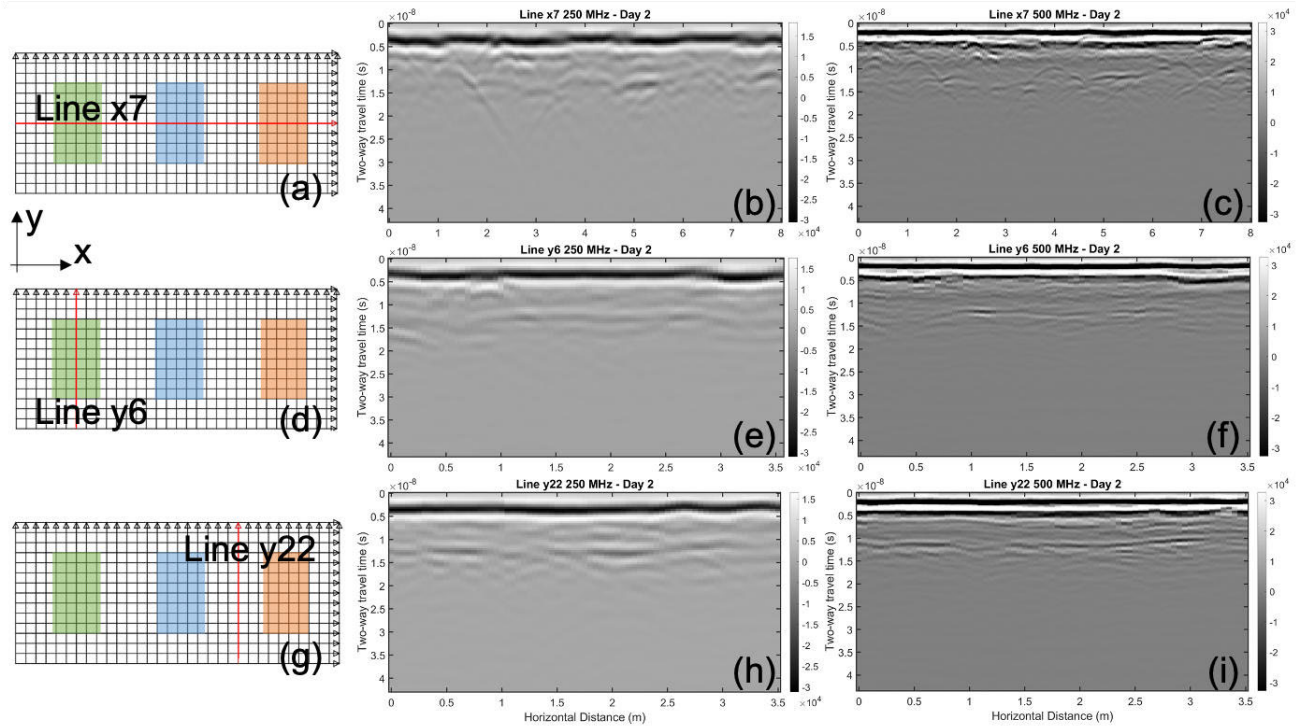

Fig. 3. Comparison of GPR radagrams recorded on Day 2 along with the NOGGIN instrument using 250 MHz antennas (b,e,h) and 500 MHz antennas (c,f,i) along (a-c) Line x7 which intersects burials A, B, C perpendicularly, (d-f) Line y6 intersecting only burial A, and (g-i) Line y22 which is parallel to Line y6 and between burials B and C. Lines x7, y6, and y22 are indicated in red colour in (a,d,g), respectively.

In Fig. 3 we show the location along three survey lines (Fig. 3a,d,g) and the corresponding GPR radargrams recorded on Day 2 with 250 MHz (Fig. 3b,e,h) and with 500 MHz (Fig. 3c,f,i) antennas using the NOGGIN instrument for Line x7, which intersects perpendicularly the three burials (Fig. 3a), Line y6 parallel and intersecting burial A (Fig. 3d), and Line y22 parallel and between burials (Fig. 3g). We can see that the data for both antenna frequencies exhibit similar features. The NOGGIN instrument at 2 ns (Fig. 4a,b) and 6 ns (Fig. 4c,d). In the 250-MHz data in Fig. 4a we can observe three very clear, high-amplitude rectangular anomalies, while in Fig. 4c we can interpret a low-amplitude rectangular anomalies corresponding with the position of burial A and a small portion of burial B. In Fig. 4b,d, i.e., for the 500-MHz data, an anomalous rectangular region corresponding with burial A is interpretable at 2 ns, while at 6 ns is very faint.

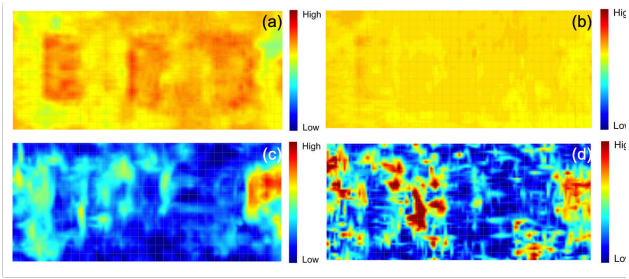

Fig. 4. Time slices at (a,b) 2 ns and (c,d) 6 ns over the complete recording grid (see Fig. 3a) recorded using the NOGGIN instrument with (a,c) 250-MHz and (b,d) 500-MHz antennas. The envelope of the data is shown to distinguish high- and low-amplitude arrivals. The colour bar shows the range of amplitudes from high to low.

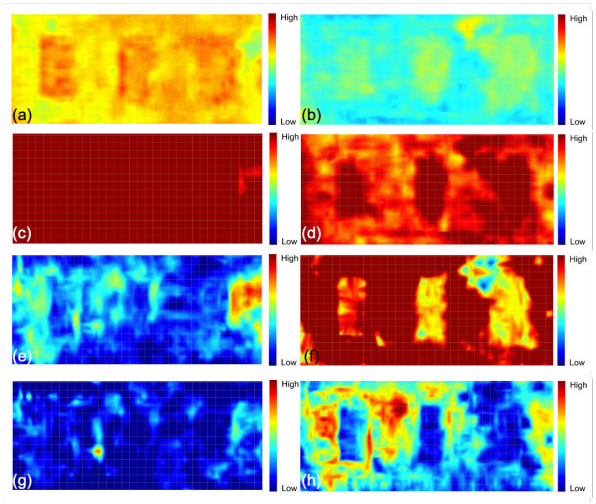

Fig. 5. Comparison of time slices extracted from data recorded with the NOGGIN instrument using 250-MHz antennas in (a,c,e,g) dry conditions (Day 1) and (b,d,f,h) wet conditions (Day 2). The extracted time slices are at (a,b) 2 ns, (c,d) 3 ns, (e,f) 6 ns, and (g,h) 7 ns. Data is enveloped to distinguish high- and low-amplitude arrivals, the colour-bar shows the range of amplitudes from high to low.

In Fig. 5 we show the comparison of measurements in dry conditions (Day 1; Fig. 5a,c,e,g) and wet conditions, i.e., after rain (Day 2; Fig. 5b,d,f,h). The data were recorded with the NOGGIN instrument using the 250 MHz antennas. We show the time slices in which we interpret anomalous features corresponding to burials A, B, C. We can observe that the time slices from Day 2, i.e., wet conditions, exhibit much clearer anomalous features with the exception of the time slice at 2 ns (Fig. 5a,b), i.e., for the shallowest depth. Both the Day 1 and Day 2 slices exhibit similar patterns at the respective times. However, the wet conditions on Day 2 in general resulted in data that exhibit slices with less clutter, which in turn allows the anomalous features to be highlighted. This can be seen in the time slices at 6 ns (Fig. 5e,f) – clear rectangular-like shapes are present in the Day 2 data (Figure 5f), and only a single shape is interpretable at the place of burial A in the Day 1 data (Figure 5e). The presence of water effectively homogenizes the soil because the water permittivity value is so much higher than that of air and soil, that many small heterogeneities disappear with the presence of water in the pore space. The fact that the soil is a marine sand is possibly helpful with reducing clutter due to increased attenuation when the soil is wet.

Next to having surveyed a grid with lines parallel or perpendicular to the main burial orientations, we also collected data at an oblique angle to see whether that would influence the outcome. Obviously, using data only along one line, it becomes more difficult to interpret burials in the data, but as can be seen in Fig.6, on the image of a grid survey the location of the burial can be estimated with greater confidence. The white dots in the left graph indicate the estimated edges based on true data. The plot again shows the instantaneous amplitude and has been filled in by Kriging interpolation.

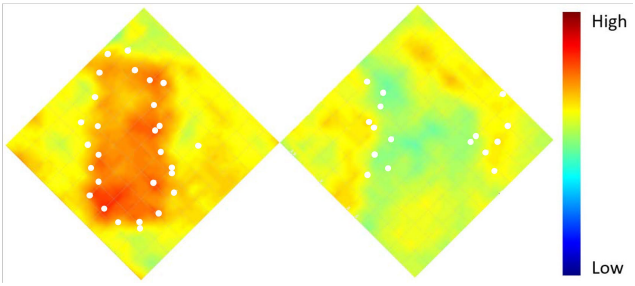

Fig. 6. Time slices at 2 ns over the rotated recording grid recorded using the NOGGIN instrument with the 250-MHz (left) and 500 MHz (right) antennas. The display is the same as described in Fig. 4.

IV. Conclusions

Having separate antennas instead of having them placed on a base plate, increases the sensitivity to surface elevation and roughness. This can be beneficial in the forensic context. Single line measurements do not provide sufficient ability to determine with confidence whether a reflective feature originates from a burial. When data is acquired on a grid, burials in sandy soil can be detected either as low or high-amplitude anomalies, depending on the situation. The line orientation is not the decisive factor for burial detection. Together, radargrams and time slices provide characteristic responses showing locations that are consistent with burials. Performing measurements before and after rainfall can be beneficial for the detectability of the presence of burials. More detailed features seem present in the data that need further investigation.

References

[1] D. W. Owsley, “Techniques for locating burials, with emphasis on the probe”, J. of Forens. Sc., vol. 40, pp. 735-740, 1995.

[2] J. J. Schultz and M. M. Martin, "Monitoring controlled graves representing common burial scenarios with ground penetrating radar"' J. Appl. Geophys., vol. 83, pp. 74-89, 2012.

[3] D. C. Nobes, “Geophysical surveys of burial sites: A case study of the Oaro Urupa”, Geophys., vol. 64, pp. 357–367, 1999.

[4] J. K. Pringle, A. Ruffell, J. R. Jervis, L. Donnelly, J. McKinley, J. Hansen, R. Morgan, D. Pirrie, and M. Harrison, “The use of geoscience methods for terrestrial forensic searches”, Earth-Sc. Rev., vol. 114, pp. 108–123, 2012.

[5] C. M. Molina, J. K. Pringle, M. Saumett, and G. T. Evans, “Geophysical monitoring of simulated graves with resistivity, magnetic susceptibility, conductivity and GPR in Colombia, South America”' Forens. Sc. Intern., vol. 261, pp. 106–115, 2016.

[6] J. K. Pringle, J. R. Jervis, , J. D. Hansen, G. M. Jones, N. J. Cassidy, and J. P. Cassella, “Geophysical monitoring of simulated clandestine graves using electrical and ground-penetrating radar methods: 0–3 years after burial”, J. of Forens. Sc., vol. 57, pp. 1467–1486, 2012.

[7] M. van Schoor, W. C. Nienaber, and A. Marais-Werner, “A controlled monitoring study of simulated clandestine graves using 3d ground penetrating radar”, Near Surf. Geophys., vol. 15, pp. 274–284, 2017.

[8] J. J. Schultz and M. M. Martin, “Controlled gpr grave research: Comparison of reflection profiles between 500 and 250 MHz antennas”' Forens. Sc. Intern., vol. 209, pp. 64–69, 2011.